Linear and Nonlinear Optical Processes Controlling S_2 and S_1 Dual Fluorescence in Cyanine Dyes

Published as part of The Journal of Physical Chemistry virtual special issue "125 Years of The Journal of Physical Chemistry".

Maryann Laboe,[#] Jurick Lahiri,[#] Nila Mohan T. M., Fangchun Liang, Benjamin G. Levine, Warren F. Beck, and Marcos Dantus*

ACCESS | Metrics & More | Article Recommendations | SI Supporting Information

ABSTRACT: We report on the changes in the dual fluorescence of two cyanine dyes IR144 and IR140 as a function of viscosity and probe their internal conversion dynamics from S_2 to S_1 via their dependence on a femtosecond laser pulse chirp. Steady-state and time-resolved measurements performed in methanol, ethanol, propanol, ethylene glycol, and glycerol solutions are presented. Quantum calculations reveal the presence of three excited states responsible for the experimental observations. Above the first excited state, we find an excited state, which we designate as S_1', that relaxes to the S_1 minimum, and we find that the S_2 state has two stable configurations. Chirp-dependence measurements, aided by numerical simulations, reveal how internal conversion from S_2 to S_1 depends on solvent viscosity and pulse duration. By combining solvent viscosity, transform-limited pulses, and chirped pulses, we obtain an overall change in the S_2/S_1 population ratio of a factor of 86 and 55 for IR144 and IR140, respectively. The increase in the S_2/S_1 ratio is explained by a two-photon transition to a higher excited state. The ability to maximize the population of higher excited states by delaying or bypassing nonradiative relaxation may lead to the increased efficiency of photochemical processes.
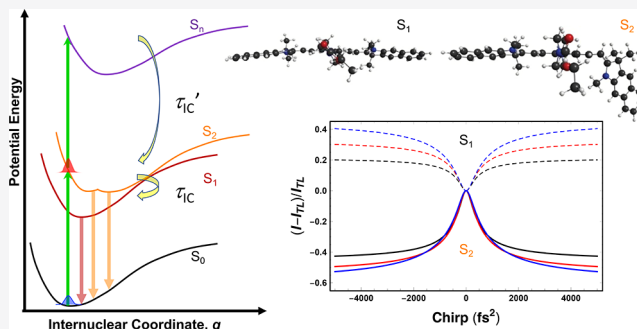
INTRODUCTION

Fluorescence from high-lying excited states is uncommon for organic molecules in solution because of the fast internal conversion (IC) to the lowest excited state of the same parity that gives rise to Kasha's rule.[1] Here, we revisit the dual fluorescence observed in cyanine dyes,[2-4] in particular, the enhanced S_2 emission observed in studies using chirped femtosecond laser pulses.[5] We endeavor to understand what leads to the unusual enhancement by restricting molecular motion via changes in solvent viscosity and shaping the laser pulses. The motivation of our work is to learn how to enable new applications of cyanine dyes through increasing the lifetime of high-lying excited states.

Cyanine dyes encompass a large category of fluorescent molecules with an odd numbered conjugated π−bonding system connecting two nitrogen atoms that branch off into a range of different substituents. Cyanine dyes are used in a wide range of applications, including bioimaging,[6-10] solar energy conversion,[11-13] photodynamic cancer therapy,[14,15] and textiles.[16] Their spectroscopic properties are easily tuned making them useful model compounds.[17] Here we focus on heptamethine cyanine dyes IR144 and IR140, shown in Figure 1, which differ in their amine substituent located in the center of

their polymethine chain. IR144 has a piperazine substituent, while IR140 has a bulky diphenylamino group. The bulky substituent gives IR140 a higher degree of steric hindrance than IR144. Notice the two configurations for IR144 and IR144′ represent the cyanine-like and bis-polar conformation of IR144, respectively; IR140 is represented in the cyanine-like conformation.[11]

When a transform-limited (TL) pulse is chirped, its pulse duration increases, and its peak intensity decreases. More importantly, the instantaneous frequency sweeps from higher to lower frequencies in a pulse with negative chirp, or from lower to higher frequencies in a pulse with positive chirp. The fast sweep of the instantaneous frequency allows one to consider a chirped pulse as using a pair of pulses with different frequencies separated by a time delay that is proportional to the chirp magnitude. This analogy, and the fact that chirped pulses lack
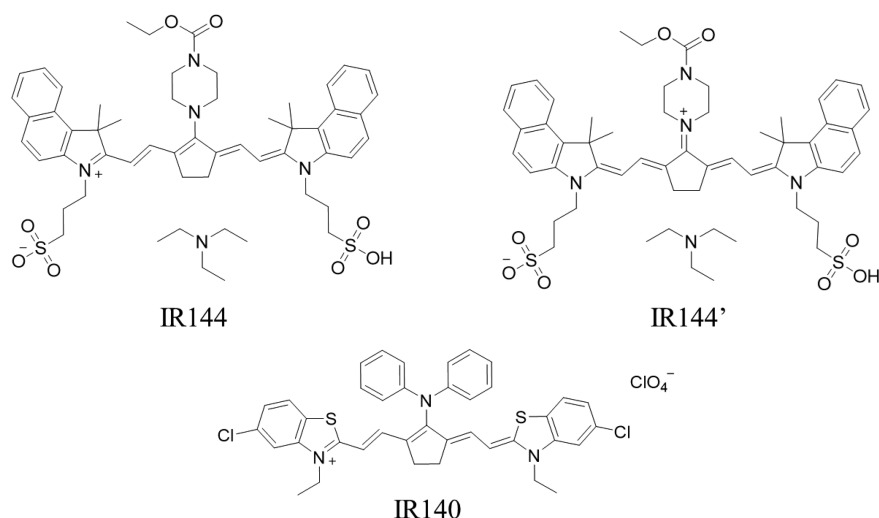
Figure 1. Cyanine-like and bis-polar conformations of IR144, and cyanine-like conformation of IR140.

time-inversion symmetry,[18] explains why chirped pulses are useful for following molecular dynamics.[19−24] The "chirp effect" following S_1 excitation consists of a decreased fluorescence yield observed for negatively chirped pulses compared with positively chirped pulses.[19,20,24,25] Experiments from our group on the excitation of the S_1 state of IR144 showed that the decrease in the S_1 fluorescence was mirrored by enhanced stimulated emission in the presence of negatively chirped pulses.[26] For positively chirped pulses, we observed enhanced S_1 fluorescence and decreased stimulated emission. Positively chirped pulses were found to be sensitive to solvation dynamics. The sensitivity of chirped-pulse measurements to solvation dynamics was sufficiently high to resolve differences in viscosity caused by ∼5% changes in the solvent temperature.[24] The changes observed in both fluorescence and stimulated emission were found to be quadratic with respect to the laser intensity even at laser intensities corresponding to 0.02% excitation probability (2 × 10^{-7} J/cm^2).[26] Nonlinear effects in laser−molecule interactions have been offered as explanations for the observation of coherent control in the "linear regime".[27,28] We have pointed out that one must first determine that the laser pulse spectrum remains unchanged as the spectral phase is changed; otherwise, changes in the spectrum can account for the observed changes in the control experiment.[29]

We explain in the following how chirped pulses interact with a molecule using the language of nonlinear spectroscopy.[30] Instead of using double-sided Feynman diagrams, we find that Albrecht wave-mixing energy-level (WMEL) ladder diagrams[31] are more instructive because one is able to show energetically why some pathways are not allowed for chirped pulses. For a review of nonlinear optical spectroscopy that includes an introduction to double-sided Feynman diagrams, ladder diagrams, and Liouville space coupling diagrams, starting from one to three field interactions which includes theory, mathematical expressions for calculating the density matrix time evolution, expected signals, and experimental results, we recommend the work of Grimberg et al.[32] We start by reminding the reader that excitation from the ground to an excited state requires two laser interactions on both the bra (represented as dashed arrows) and ket (represented by solid arrows) to bring the ground state to the excited state, thus creating a population. The population in the excited state following such linear interaction is proportional to

$$P_{1 \leftarrow 0} \propto |\langle e|\mu \cdot E(t)|g\rangle|^2 = \langle e|\mu \cdot E(t)|g\rangle\langle g|\mu \cdot E(t)^*|e\rangle \quad (1)$$

where μ is the transition dipole, and $E(t)$ is the complex time-dependent field. In the diagrams shown in Figure 2, we include
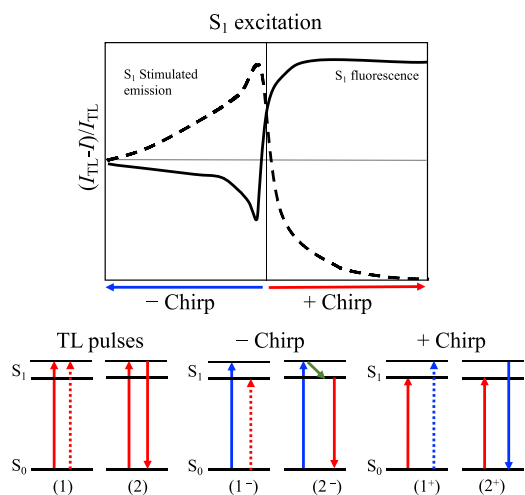

Figure 2. Interaction of chirped laser pulses with the S_1 state of a molecule. (top) Relative changes in fluorescence and stimulated emission from the S_1 state as a function of chirp (bold line and dashed line, respectively), according to ref 24. (bottom) Albrecht ladder diagrams representing the laser-molecule interaction for TL and chirped pulses. Pathways (1^-) and (1^+) are independent of chirp, pathway (2^-) is responsible for the enhanced stimulated emission and decrease in fluorescence. Pathway (2^+) causes no effect because it is energetically forbidden. Solid/dashed arrows indicate ket/bra interactions. Blue/red arrows indicate the high/low frequency portion of the spectrum. Green arrows indicate nonradiative transitions including wave packet motion.

only two electronic states S_0 and S_1. Excitation of the S_1 state with chirped pulses, as we have done for IR144,[24] and shown in Figure 2, we observe that fluorescence is depleted for negative chirp values but enhanced for positive chirp values. When using TL pulses, the ladder diagram for pathway (1) in Figure 2 populates the excited state, while pathway (2) stimulates emission back to the ground state.

When using chirped pulses, we find that pathways (1^-) and (1^+) are independent of the timing between higher and lower

energy portions of the pulse (i.e. independent of phase). Both pathways create a population in the excited state that is independent of chirp. For negatively chirped pulses, however, the higher energy portion of the pulse (blue arrow) interacts first with the ket, and then the lower energy portion of the pulse (red arrow) interacts with the bra, as shown in pathway (2^-). Hence, there is no net population created in the S_1 state. This explains the reduction in observed fluorescence and justifies the observation of enhanced vibrational coherence following negative chirp pulse excitation.[33,34] Pathway (2^+) for positively chirped pulses cannot take place for energetic reasons (compare with pathway (2^-)). In summary, these diagrams (and their complex conjugates) explain the observed dependence of fluorescence and stimulated emission as a function of pulse chirp sign and magnitude as shown in Figure 2. Here we have illustrated the cases for two field interactions. One may add a third interaction to simulate higher-order processes; however, it is clear that the outcome will depend on the first two interactions shown here and their complex conjugates.

When chirp-dependence experiments were carried out on the S_2 excited state of IR144 and IR806, we found a very different molecular response, illustrated in Figure 3.[5] The maximum S_2
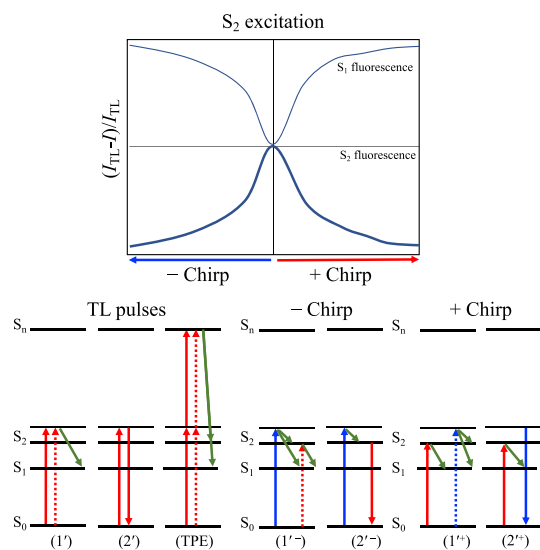

Figure 3. Interaction of chirped laser pulses with the S_2 state of a molecule. (top) Relative changes in fluorescence from the S_1 and S_2 states, (light and bold lines, respectively) as a function of chirp, according to ref 5. (bottom) Albrecht ladder diagrams representing the laser-molecule interaction for TL and chirped pulses. Pathway (TPE) where two-photon excitation to an upper excited state S_n is accessible in this case, leading to enhanced S_2 fluorescence. Pathways $(1'^-$ and $1'^+)$ are independent of chirp. Pathway $(2'^-)$ is responsible for a decrease in fluorescence observed for negative chirp; however, nonradiative relaxation via IC leads to decreased S_2 fluorescence that is essentially symmetric with chirp sign. Solid/dashed arrows indicate ket/bra interactions. Blue/red arrows indicate the high/low frequency portion of the spectrum. Green arrows indicate nonradiative transitions including wave packet motion.

fluorescence was observed for TL pulses, while a decrease in fluorescence was found for both negatively or positively chirped pulses. In this work, we revisit this unusual behavior. The chirp dependence of the S_2 state's fluorescence is illustrated in Figure 3, where in addition to the laser-matter interactions, we show nonradiative relaxation from the different states using solid green arrows. At first glance, we find that the pathways relevant

to S_1 excitation are identical to those involving S_2 excitation. However, there are two main differences. First, the pathway responsible for two-photon excitation (TPE) becomes available only for TL pulse excitation, provided that there is a state resonant with two-photon excitation, since the field and laser intensity is sufficiently high. Second, each excitation to S_2 is now competing with faster relaxation because of the excitation taking place in a higher density of states' region and because of IC to S_1. Like the case for S_1 excitation, pathways $(1'^-)$ and $(1'^+)$ are independent of the timing between higher and lower energy portions. Like for S_1 excitation, pathway $(2'^-)$ leads to a decrease in S_2 population. The main difference in these pathways is the presence of fast relaxation that includes IC to S_1, as indicated by the green arrows. These processes compete with optical excitation and result in signals that are almost symmetric as a function of chirp. A greater degree of asymmetry was observed in mesopiperidine-IR806 (mPi-IR806).[5] As a result of these laser−matter interactions, we expect that chirped pulses result in a lower S_2 population but higher S_1 population. TL pulses result in higher S_2 and lower S_1 population because IC from S_2 to S_1 is relatively slow in these cyanine molecules and because a higher excited state, indicated by S_n, is resonant with the laser excitation.

Here we use femtosecond chirped pulses to better understand the time-correlated wave packet motion that leads to IC considering linear and nonlinear light-molecule interactions. We combine chirp control and the dependence of the rate of IC on solvent viscosity[35−37] to explore in greater detail the role of intramolecular structural changes required in cyanine dyes to enable IC. The goal of our experiments is to achieve the largest S_2/S_1 ratio to enable novel photochemistry, solar energy capture, and perhaps photodynamic therapy applications.

The organization of the paper is as follows: First, we describe the experimental details including steady-state spectroscopy, lifetime measurements, and chirp-dependent measurements. Second, we present steady-state spectroscopy of the two cyanine dyes in different solvents along with lifetime measurements. Third, we show chirp-dependent measurements for different solvents obtained at different laser intensities. Fourth, we present quantum chemistry calculations performed on both molecules that identify the different excited states involved as well as their equilibrium configurations. Fifth, we present a kinetic model for the observed chirp dependence. Finally, we discuss how our experimental findings, quantum calculations, and a kinetic model come together to validate our conclusions.

■ EXPERIMENTAL DETAILS

IR144 and IR140 (Exciton, CAS Nos.: 54849-69-3 and 53655-17-7) were purchased and used without further purification. We assume that the presence of the triethylamine 1:1 in IR144 does not affect the results presented given the complete solvation of the dye and the low concentrations used here. Spectrophoto-metric-grade methanol, ethanol, *n*-propanol, ethylene glycol, and glycerol were purchased from Sigma-Aldrich. Solutions made with ethylene glycol and glycerol were prepared by first dissolving the dye in 1 part methanol and then combined with 19 parts of the respective solvent. The results presented were obtained with 50 μM concentration. Measurements were repeated with different concentrations ranging from 25 to 2.5 μM concentrations, although the signal-to-noise ratio was poor at lower concentrations.

Steady-state spectroscopy measurements were carried out in 1 cm path length quartz cuvettes, with UV antireflection-coated

windows on all four sides. Absorption, fluorescence with excitation at 522 nm, and excitation emission matrix (EEM) spectra were collected using a Horiba Duetta Spectrometer. All measurements were taken at room temperature (~294 K).

Fluorescence lifetime measurements were acquired following excitation from a picosecond pulsed laser with a repetition rate of 80 MHz centered at 531 nm (LDH-P-FA-530XL, Picoquant). A half-wave plate was used to ensure the vertical polarization of the excitation beam. The IR144 and IR140 solutions were contained in a 1 cm cuvette. Fluorescence emission collected perpendicular to the laser beam was analyzed at parallel and perpendicular polarizations with respect to the vertical polarization of the excitation pulse by a polarizer. Detection was carried out with a 16-photomultiplier time-correlated single-photon counting (TCSPC) system (SPC-830 TCSPC, Becker-Hickl, GmBH). The decay times correspond to the isotropic component of the fluorescence decays. Iterative reconvolution of the fluorescence decays was carried out to obtain the decay lifetimes; the instrument response function (IRF) width was on the order of 130 ps.

Chirp experiments were carried out using a Spectra−Physics Spirit-NOPA-3H noncollinear optical parametric amplifier (NOPA) pumped by the third harmonic (347 nm) of a 1040 nm Spectra−Physics Spirit-4W amplified Yb laser operating at a repetition rate of 100 kHz. The NOPA was tuned to generate laser pulses centered at 522 nm. Laser pulses were sent into the femtoJock P (Biophotonic Solutions, part of IPG Photonics) pulse shaper. The chirp magnitude φ_2 is controlled in the frequency domain by programming the pulse shaper to introduce the spectral phase function $\varphi(\omega) = 0.5\varphi_2(\omega - \omega_0)^2$, where ω_0 is the carrier frequency of the laser pulse.

Multiphoton intrapulse interference phase scan (MIIPS) was first used to automatically compress the pulses to their TL duration,[38,39] In addition, we optimized the laser fidelity,[40] which is a measure of the pulse-to-pulse spectral phase and amplitude variability of the laser pulses. Pulse compression was done using a thin beta-barium borate (BBO) second harmonic generation (SHG) crystal that was placed in the same location where the sample would be placed. Pulse durations of 25 fs were used for all experiments. During the MIIPS scans, a quartz cuvette face was placed in the beam path to compensate for dispersion generated by the quartz cuvette wall when the sample is in place. The pulse energy was 200 nJ for IR144 experiments and around 50 nJ for IR140 experiments. The pulse energies ranged from 50 to 150 nJ during power-dependence experiments. An antireflective 10 cm focal length lens focused the pulses into the front of the quartz cuvette that held each sample. A multimode optical fiber was held perpendicular to the excitation beam at the location of the laser focus. The optical fiber carried the fluorescence to a QE Pro Spectrometer (Ocean Optics), and the spectra were collected by the MIIPS software and recorded. The QE spectrometer wavelength calibration was based on atomic lines emitted by a mercury lamp. The intensity calibration was accomplished by comparing fluorescence spectra obtained by the QE spectrometer and fluorescence spectra of the same solution acquired by a calibrated Duetta spectrometer. The Duetta spectrometer intensity calibration was based on the wavelength dependence of the Raman line of water. We found both that intensity calibration was very important given that the S_1 state of these dyes emits at wavelengths ranging from 800−1100 nm and that the wavelength range is outside the detection capability of photomultipliers and near the long-wavelength edge of silicon detectors. Chirp was introduced to the pulses

using the pulse shaper. The chirp range over which fluorescence was collected was −5000 fs^2 to +5000 fs^2. The entire chirp range was divided into 300 fs^2 steps. At least 5 measurements were taken at each step for each of the 10 samples. Each measurement corresponded to 3 averages with an integration time of 50 ms for methanol, ethanol, and propanol solutions and 300 ms for ethylene glycol and glycerol solutions.

■ RESULTS

Steady-state absorption and fluorescence spectra of IR144 and IR140 in methanol, ethanol, n-propanol, ethylene glycol, and glycerol are shown in panels a and b, respectively, of Figure 4.
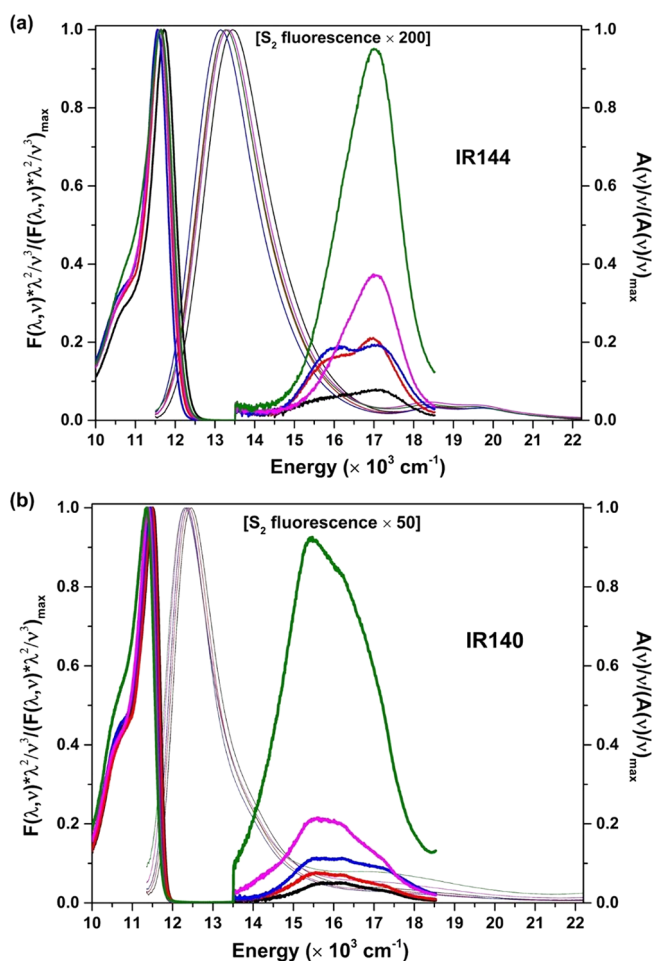

Figure 4. Steady-state absorption and fluorescence spectra for (a) IR144 and (b) IR140. The normalized absorption of both IR144 and IR140 is represented with thin lines, whereas the normalized emission is shown with thicker lines. Methanol, ethanol, n-propanol, ethylene glycol, and glycerol are represented by black, red, blue, pink, and green lines, respectively.

These spectra are plotted as the transition dipole (or oscillator) strength.[41,42] The absorption dipole strength was calculated by dividing the absorption value by its respective wavenumber $A(\nu)/\nu$. Fluorescence spectra were converted to wavenumber, multiplied by the wavelength squared, and divided by the respective wavenumber cubed to calculate the fluorescence dipole strength $F(\nu)/\nu^3$.[41,42] The lower-energy S_0 to S_1 transition absorption band is centered around 13 500 and 12 800 cm^{-1} for IR144 and IR140, respectively. The higher energy S_0 to S_2 absorption bands are associated with two

configurations that we will refer to as S_2^L and S_2^H according to their lower- or higher-energy transitions, respectively. The S_0 to S_2 absorption bands are ~18 210 and 19 710 cm^{-1} for IR144, and ~17 960 and 19 510 cm^{-1} for IR140. The emission spectra for IR144 and IR140 following excitation at 19 157 cm^{-1}, accessing the higher S_2 excited electronic state configuration, show three emission bands. The fluorescence bands associated with S_2^L and S_2^H for IR144 are at 15890 and 17150 cm^{-1}, respectively, while those for IR140 are centered at 15900 and 17230 cm^{-1}. The S_1 emission is centered at 11,750 cm^{-1} for IR144 and 11,500 cm^{-1} for IR140.

IR144 shows a solvatochromic shift for both the absorption and fluorescence of the S_1 excited state that is not linear with viscosity. Propanol gives the largest redshift, with respect to methanol, even though glycerol has the highest polarity. Both solvent viscosity and polarity play a role in IR144 absorbance and emission band positions. Similarly, IR140 shows a solvatochromic shifts for both absorption and fluorescence spectra as a function of viscosity. The S_0 to S_2 absorbance increases with solvent viscosity. For both molecules, as solvent viscosity increases, the overall S_2/S_1 fluorescence ratio increases. Following excitation of S_2, emission from S_2^H is favored by IR144, whereas emission from S_2^L is favored by IR140.

As can be observed in Figure 4, the intensity of the S_2 emission increases with solvent viscosity. In Figure 5, we plot the S_2/S_1 ratio as a function of solvent viscosity for both IR144 and IR140.
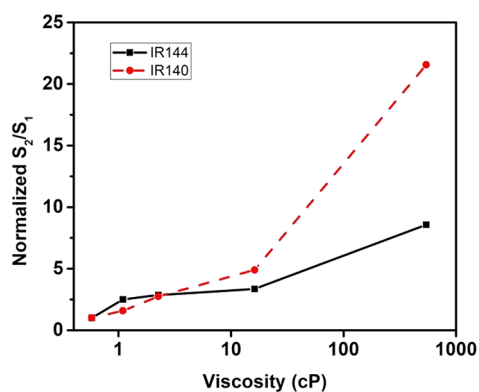

Figure 5. Integrated fluorescence ratio of S_2/S_1 from steady-state spectra for IR144 and IR140 as a function of varying solvent viscosity (logarithmic scale). The numbers have been normalized such that the ratios are 1 for the respective methanol samples.

EEM spectra, which record the steady-state fluorescence emission intensity as a function of excitation wavelength in a 2D contour map, were collected for both IR144 and IR140 (Figure 6a,b). The 14 085−22 000 cm^{-1} emission region has been enhanced by a multiplication factor of 1200 (for IR 144) and 350 (for IR140). The EEM spectra makes it clear when the S_1 and S_2 excited states are reached. We also note that excitation in the 14 000−16 200 cm^{-1} region for IR144 and the 13 500−15 200 cm^{-1} region of IR140, leads to bright emission from S_1, likely indicating the presence of an excited state that quickly relaxes to S_1.

Fluorescence lifetime measurements, with an excitation wavelength of 18 832 cm^{-1}, were carried out in IR144 and IR140 solutions in methanol, ethylene glycol, and glycerol. Figure 7a,b show fluorescence lifetime measurements from IR144 S_2 and S_1 states, respectively. The population from S_2 decays via IC to S_1 and fluorescence to S_0. However, the presence of these two decay pathways should lead to a single exponential decay with a rate corresponding to the sum of both pathways. The presence of a biexponential decay indicates that a fraction of the population remains in S_2. As we will discuss later in the manuscript, we identify a change in the molecular structure in the S_2 state as a bottleneck that prevents IC to S_1. The molecules that undergo the configuration change have a much slower IC to S_1 and primarily exhibit $S_2 \rightarrow S_0$ fluorescence. The addition of a non-IC configuration to S_2 results in the biexponential fluorescence decay observed. The S_1 emission signal shows a rise followed by a decay, with both lifetimes increasing with solvent viscosity. Figure 8a,b show fluorescence lifetime measurements for S_2 and S_1 states, respectively, for IR140. The S_2 fluorescence lifetime increases with viscosity for IR140 and IR144. Interestingly, the IR140 S_1 fluorescence lifetime does not follow the same viscosity trend. We find the fluorescence lifetime for IR140 in methanol to be similar to that in glycerol. The deconvoluted fluorescence lifetime values are presented in Table 1.

Femtosecond chirp scans, from negative chirp values (higher before lower frequencies) to positive chirp values (lower before higher frequencies) were carried out on IR144 and IR140 in methanol, ethanol, and propanol. The chirp applied to the excitation pulse, with a near Gaussian spectrum and a central wavelength near the S_2 absorption band, for both IR144 and IR140, is scanned as the fluorescence spectra spanning both excited states are collected. Figure 9a,b show the trend in S_1 and
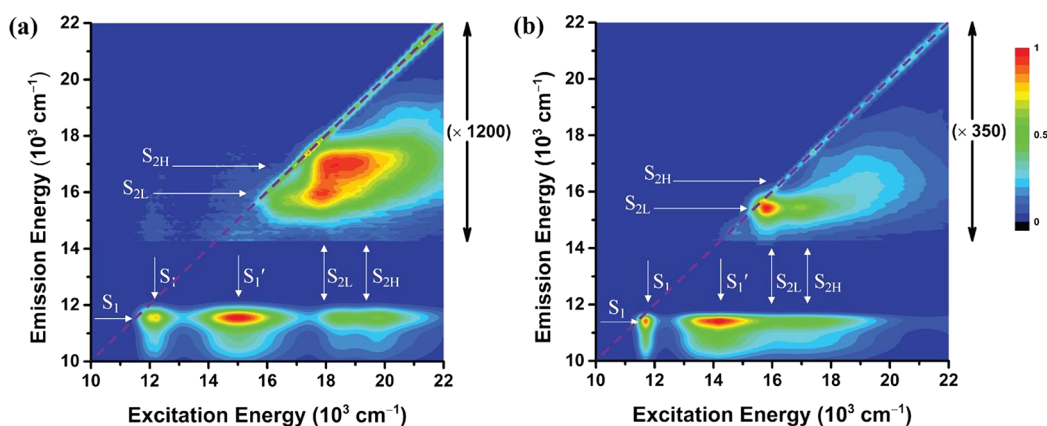

Figure 6. Excitation emission matrix spectra of (a) IR144 and (b) IR140 in *n*-propanol. The diagonal indicates scattered excitation light when both excitation energy and emission energy are equal.
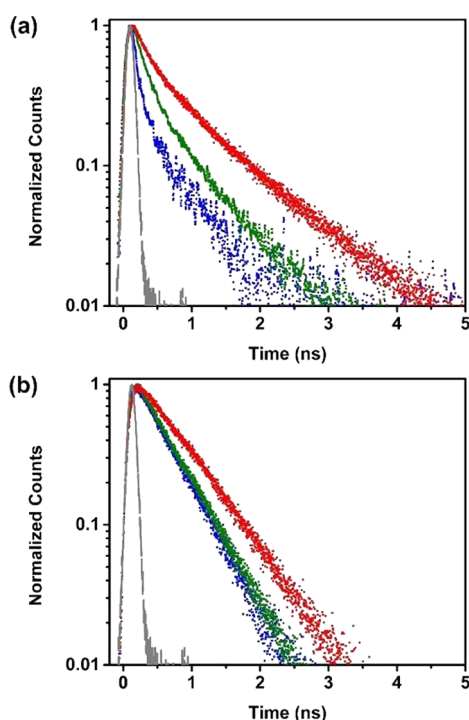
Figure 7. Fluorescence decay of IR144 detected at (a) $S_2 \rightarrow S_0$ fluorescence maxima and (b) $S_1 \rightarrow S_0$ fluorescence maxima in methanol (blue dots), ethylene glycol (green dots), and glycerol (red dots). The fluorescence lifetimes for (a) have been obtained from the function $f(t) = a_1 \exp(-t/\tau_1) + a_2 \exp(-t/\tau_2)$, while for (b), they have been obtained from the function $f(t) = -b_1 \exp(-t/\tau_3) + b_2 \exp(-t/\tau_4)$. The time constants have been obtained post deconvolution of the IRF from the fluorescence decay signals. In both cases, the preexponential components are such that ($a_1 + a_2 = 1$ and $b_1 + b_2 = 1$).
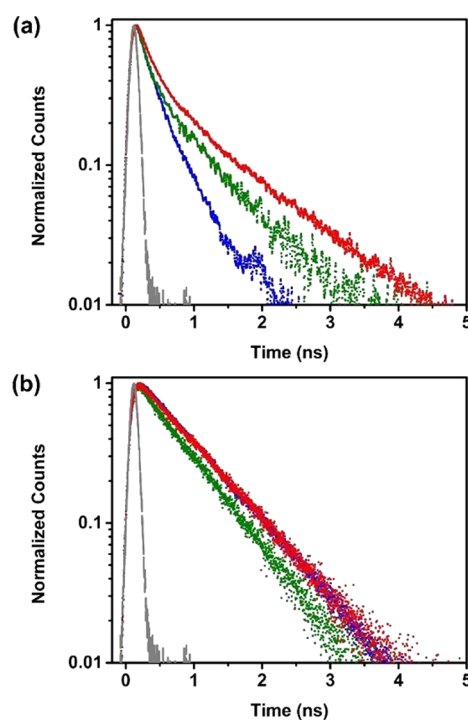

Figure 8. Fluorescence decay of IR140 detected at (a) $S_2 \rightarrow S_0$ fluorescence maxima and (b) $S_1 \rightarrow S_0$ fluorescence maxima in methanol (blue dots), ethylene glycol (green dots), and glycerol (red dots). The fluorescence lifetimes for (a) have been from the function $f(t) = a_1 \exp(-t/\tau_1) + a_2 \exp(-t/\tau_2)$, while for (b), they have been obtained from the function $f(t) = -b_1 \exp(-t/\tau_3) + b_2 \exp(-t/\tau_4)$. The time constants have been obtained post deconvolution of the IRF from the fluorescence decay signals. In both cases, the preexponential components are such that ($a_1 + a_2 = 1$ and $b_1 + b_2 = 1$).

S_2 integrated fluorescence with increasing chirp for IR144 and IR140, respectively. The y-axis is the relative change in integrated fluorescence, with respect to TL fluorescence.

As shown in Figure 9, and similar to previous experiments from our group,[5] the resulting increase in S_2 and decrease in S_1 fluorescence at near zero chirp are nearly symmetrical with respect to chirp magnitude. This chirp dependence is unusual. As mentioned in the Introduction, excitation with negatively chirped pulses should lead to a pronounced decrease in fluorescence compared with excitation with positively chirped pulses. It is important to note that the total integrated S_1 fluorescence is considerably higher than the total integrated S_2 fluorescence (see Figure 2). The shaded gray outlines, located on the bottom half of Figures 9a,b, represent the SHG dependence as a function of chirp obtained with the experimental pulses. The SHG intensity is proportional to the inverse of the pulse duration of the chirped pulses, τ_{out}, as given by eq 2. In this equation, τ_{in} is the input pulse, $f = 4*\ln2$, and φ_2 is the amount of chirp.

$$\tau_{out} = \tau_{in}\sqrt{1 + f^2\left(\frac{\varphi_2}{\tau_{in}^2}\right)^2} \tag{2}$$

Because the observed response to chirped pulses following S_2 excitation in cyanines is unusual, we have extended our previous work to solvents with higher viscosity values using methanol, ethanol, and propanol solutions. We find that as the viscosity increases, the effect that chirped pulses elicits on the

fluorescence increases in magnitude, for both S_1 and S_2. In IR144, the same chirp dependent symmetrical S_2/S_1 enhancement for TL pulses is apparent for each solvent. For IR140, the S_2/S_1 ratio increase is observed near zero chirp, but the dynamics observed are less symmetric with respect to chirp. We note a slight increase in S_1 and S_2 emission for positively chirped pulses, as compared with negatively chirped pulses. The lower fluorescence for negatively chirped pulses is reminiscent of the chirp dependence observed in first excited states showing depleted fluorescence for negatively chirped pulses due to stimulated emission (see Figure 2).[19−24] One can understand the asymmetry by considering a negatively chirped pulse experiment as the one in which a higher frequency pulse launches the wave packet in the S_2 excited and a lower frequency pulse brings the wave packet back to the ground state.

One can get a sense of the wave packet motion in the S_2 state using eq 1 to calculate an effective pulse duration corresponding to the delay between the blue and red frequency components, where τ_{in} is the laser pulse duration when TL. This was done to calculate the values in fs listed on the top x-axis of Figures 9 and 10. The broadening of the chirp dependence measured for different solvents implies that the first 50−200 fs regime is associated with motion of a wave packet away from the FC region toward IC or toward the equilibrium geometry of the S_2 state, depending on the solvent. We can get a sense of the delayed wave packet motion in the different solvents by taking the inverse of eq 1 and adding fitting parameters h and b, the amplitude and baseline, to obtain eq 3. This equation is then used to fit the experimental S_2 chirp dependence curves obtained

Table 1. Fluorescence Lifetimes Obtained from Time-Correlated Single Photon Counting Experiments[a]

molecule	solvent[b]	a_1	τ_1 (ps)	τ_2 (ps)	b_1	τ_3 (ps)	τ_4 (ps)
IR144	MeOH	0.86	46 ± 1	452 ± 10	0.07	32 ± 3	455 ± 2
	EG	0.78	175 ± 2	682 ± 14	0.05	43 ± 3	456 ± 1
	Gl	0.60	221 ± 4	932 ± 13	0.05	48 ± 3	630 ± 2
IR140	MeOH	0.52	107 ± 3	347 ± 5	0.03	44 ± 1	730 ± 2
	EG	0.71	124 ± 2	687 ± 9	0.06	26 ± 1	617 ± 2
	Gl	0.69	174 ± 2	914 ± 11	0.03	42 ± 1	726 ± 2

[a]The time constants are as defined in Figures 7 and 8. [b]Abbreviations: MeOH = methanol, EG = ethylene glycol, Gl = glycerol.
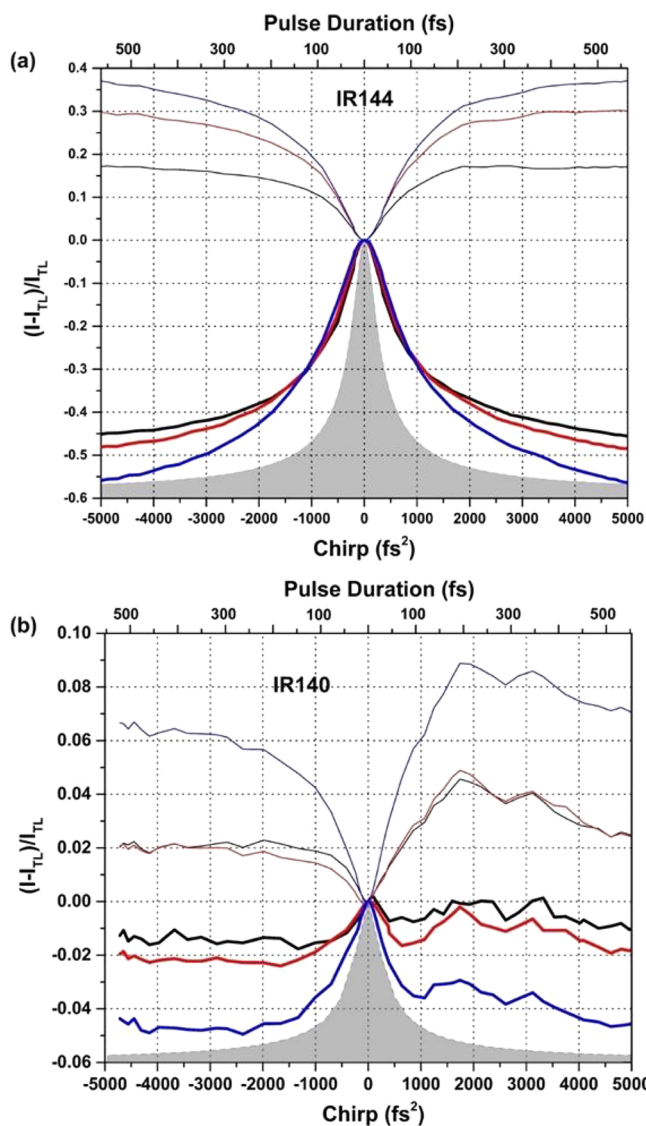

Figure 9. Chirp dependence scans conducted on (a) IR144 and (b) IR140 from −5000 fs^2 to +5000 fs^2 at constant laser power for each molecule. A lower laser power intensity was used for IR140. The thinner and thicker lines show the relative fluorescence intensity as a function of chirp compared to its TL value $(I−I_{TL})/I_{TL}$ for S$_1$ and S$_2$, respectively. Methanol, ethanol, and n-propanol are represented by black, red, and blue lines, respectively.

Figure 10. Chirp dependence scans carried out as a function of laser intensity for (a) IR144 and (b) IR140 in methanol. The thinner and thicker lines show the relative fluorescence intensity as a function of chirp compared to its TL value $(I−I_{TL})/I_{TL}$ for S$_1$ and S$_2$, respectively. Laser excitation power of 15, 10, and 5 mW are represented by black, red, and blue lines, respectively.

for the different solvents in Figure 9a to obtain a fitting parameter τ_c that is then used to calculate changes in the wave packet dynamics. When $\tau_c = \tau_{in}$, we recover the experimental SHG intensity dependence. When the radical in the denominator equals 2, it implies that the chirped pulse has doubled in duration; and from then on, pulse duration increases
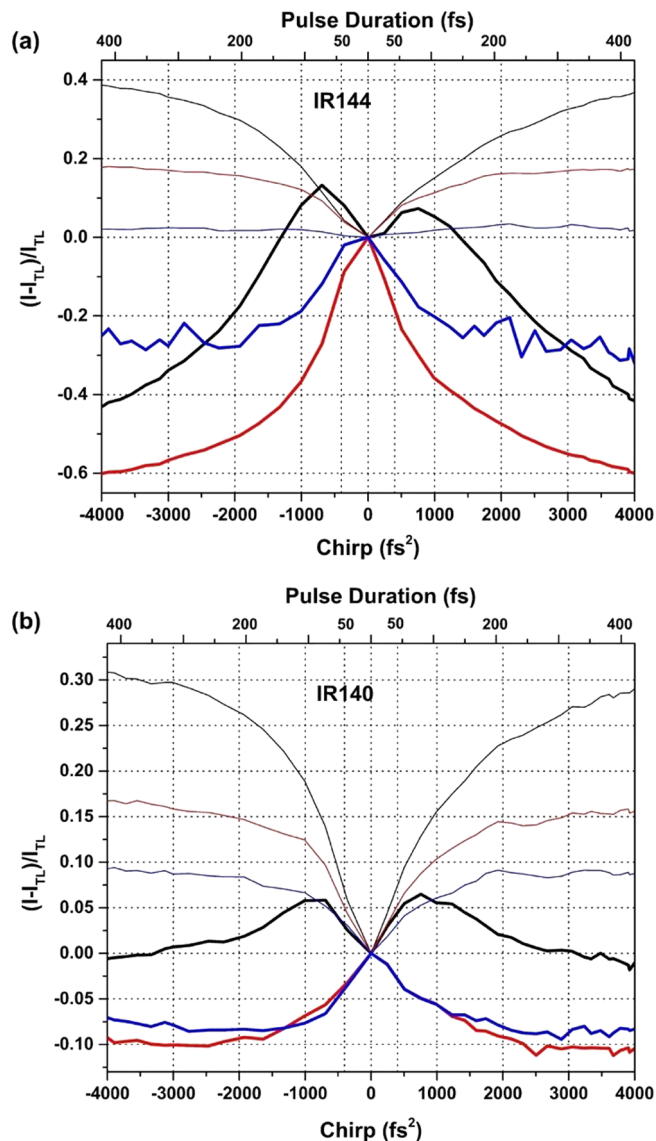
linearly with chirp. We have chosen this point, when a chirped pulse can be considered analogous to two separate pulses with different central frequency, to define the "wave-packet motion" time, a parameter that is proportional to the initial wave packet displacement. The resulting parameters, along with a "wave-packet motion" obtained by solving eq 3 for each of the τ_c values

when $b = 0$ and $h = 1$ and setting $y = 1/2$, are listed in Table 2. The values reflect the delayed wave packet motion in the

Table 2. Fitted Chirped S_2 Fluorescence Curves Were Fitted with a Lorentzian Line-Shape

molecule	solvent	τ_c (fs)	error	wave-packet motion (fs)[a]
IR144	methanol	35.3	±0.4	90
	ethanol	38.3	±0.36	105
	n-propanol	43.4	±0.34	133

[a]The wave packet motion time is calculated by solving eq 3 for the given τ_c values.

different solvents resulting from the increased viscosity forming a solvent cage, which prevents large amplitude motion.

$$y = b + \frac{h}{\sqrt{1 + f^2 \left(\frac{\varphi_2}{\tau_c^2}\right)^2}} \tag{3}$$

Power-dependence experiments were conducted for methanol solutions of both dyes, as shown in Figures 10a,b. With the increase in laser power the S_2 intensity appears to saturate for both dyes at a laser power of 15 mW. At the highest intensity, maximum S_2 emission is no longer observed for TL pulses. Notice that saturation is not observed for S_1 fluorescence. We find the observed chirp dependence of the S_2 state in IR144 is significantly greater than the effect observed in IR140.

Having shown that viscosity causes a higher S_2/S_1 emission ratio in both IR144 and IR140, especially for TL pulses, we explore a possible relationship with chirp and laser intensity on the S_2 emission spectra of the molecules (Figure 11a,b). Measurements were repeated for three laser powers, 10, 15, and 20 mW. The pulses were TL (black), positively (red) or negatively (blue) chirped. For IR144, when excited by TL pulses, we find that the three intensities produce the same spectrum which corresponds to S_2^H. For chirped pulses, we find that the blue-shifted S_2^H emission is less intense but increases with laser pulse intensity. This trend is not observed in IR140 (Figure 11b); in fact, 10 and 15 mW excitation with TL and chirped pulses produced identical spectra. This is consistent with IR140 preferring emission from the S_2^L configuration.

The motivation of this work is to maximize the lifetime of S_2 by preventing or delaying IC to S_1 so that the excess energy is available for photochemical processes such as solar energy capture or therapeutic applications. Therefore, we quantify the integrated S_2/S_1 fluorescence ratio observed for IR144 and IR140 in the different solvents by steady-state fluorescence spectroscopy as well as by femtosecond TL and chirped pulses in Table 3. Increasing solvent viscosity increased the S_2/S_1 ratio by a factor of 8.6 and 21 for IR144 and IR140, respectively. Femtosecond TL pulses caused an even higher enhancement in the S_2/S_1 ratio, by a factor of 39 and 47 for IR144 and IR140, respectively. When comparing the change in the S_2/S_1 ratio obtained for femtosecond chirped pulses for methanol and TL pulses for glycerol, we obtain an overall effect of 86 and 55 for IR144 and IR140, respectively. The large difference in the effect observed for femtosecond pulse excitation compared with steady-state spectroscopy indicates an additional pathway for the excitation that populates S_2, as will be discussed below.
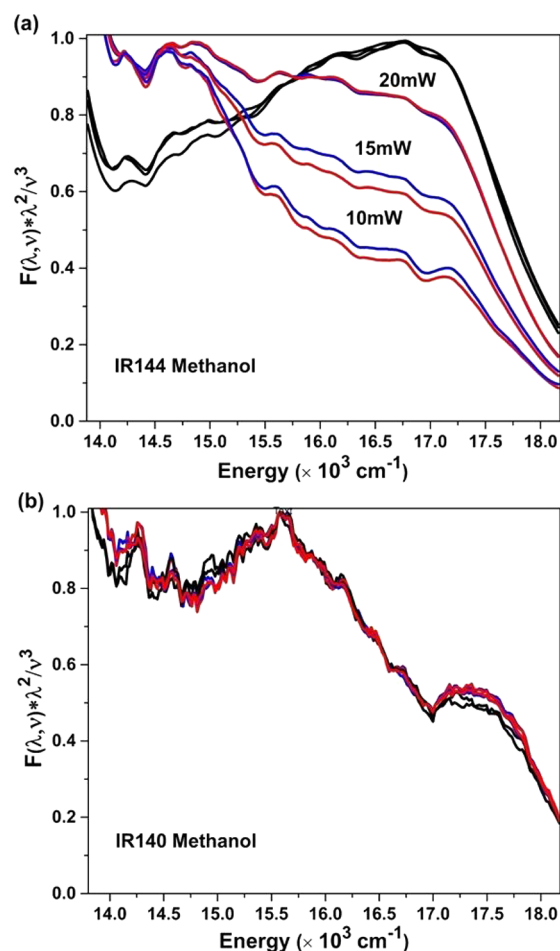

Figure 11. Normalized S_2 fluorescence spectra are plotted as a function of chirp and average laser power for (a) IR144 and (b) IR140. The blue line (positive chirp) averages the fluorescence spectrum for chirp values from +4000 fs^2 to +5000 fs^2, while the red line (negative chirp) averages the fluorescence spectrum for chirp values from −4000 fs^2 to −5000 fs^2. The black line presents the spectra for transform-limited pulses, which stay relatively the same as the power increases for both dyes. For (b) IR140, the S_2 fluorescence spectrum is not dependent upon chirp or laser power.

Table 3. S_2/S_1 Integrated Fluorescence Intensity Ratios

molecule	solvent	viscosity (cP)[43−47]	steady state	TL pulses	chirped pulses
IR144	methanol	0.579	0.0014	0.022	0.010
	ethanol	1.164	0.0035	0.0342	0.013
	n-propanol	2.197	0.0040	0.045	0.015
	ethylene glycol	17.3	0.0047	0.030	0.025
	glycerol	543	0.012	0.86	0.82
IR140	methanol	0.579	0.0051	0.027	0.023
	ethanol	1.164	0.0081	0.023	0.021
	n-propanol	2.197	0.014	0.028	0.025
	ethylene glycol	17.3	0.025	0.10	0.10
	glycerol	543	0.11	1.27	1.19

■ THEORY

Time-dependent density functional theory (TD-DFT) calculations were performed to identify the absorption and emission transitions of IR140 and IR144 molecules. Though TD-DFT
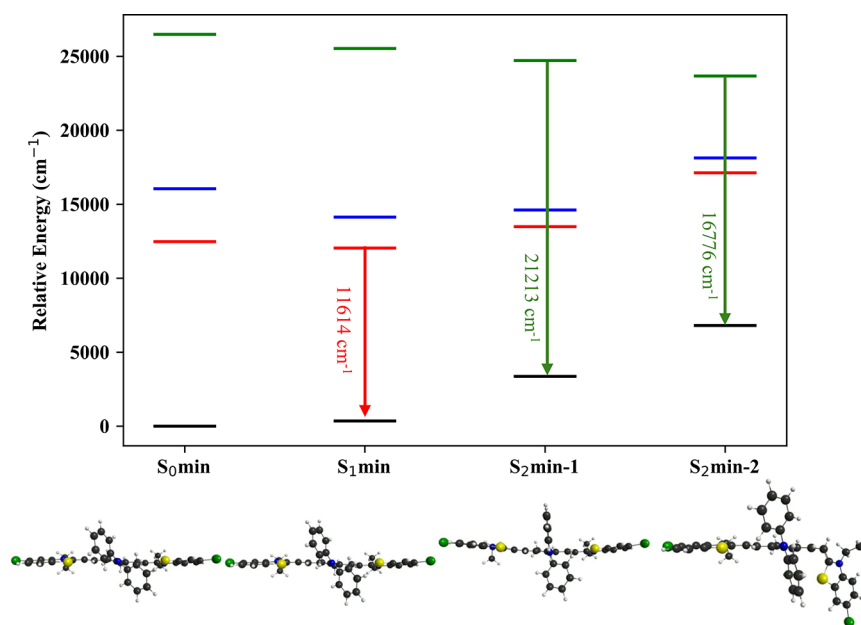
Figure 12. Computed state energies of IR140 in glycerol at corresponding geometries. S_0, S_1, S_1', and S_2 energies are shown by black, red, blue, and green lines, respectively. Energies for S_1, S_1', and S_2 are shifted as described in the text.
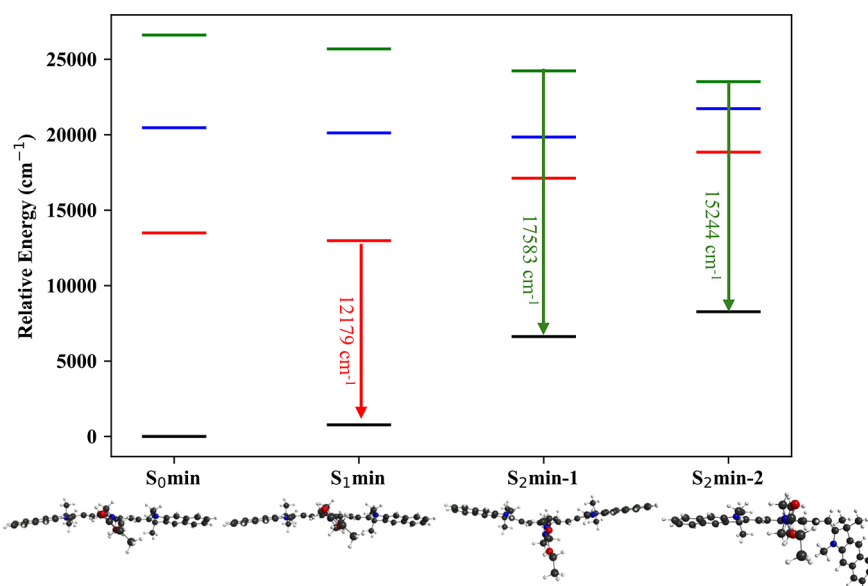

Figure 13. Computed state energies of IR144 in glycerol at corresponding geometries. S_0, S_1, S_1', and S_2 energies are shown by black, red, blue, and green lines, respectively. Energies for S_1, S_1', and S_2 are shifted as described in the text.

calculations are known to predict excitations energies with errors of several tenths of an eV in cyanine dyes, the shapes of potential energy surfaces are typically found to be very accurate.[48,49] All calculations were performed with the TeraChem software package.[50−52] Geometries were optimized at the CAM-B3LYP[53]/6-31G* level. Except where noted otherwise, all calculations were performed using an implicit model of the glycerol solvent (conductor-like polarizable continuum model, C-PCM,[54,55] with a dielectric constant $\varepsilon = 46.5$). All calculations were repeated in implicit methanol ($\varepsilon = 33.0$), with effectively identical results, except as noted specifically below. Alkyl chains over three carbons long and any associated sulfonate groups were replaced by methyl groups to save computational expense. Ground state optimizations show that the s-*trans* conformers have a lower ground state energy than the s-*cis* conformers for

both molecules. In both molecules, the central amine group was found to rotate out of the plane of the polymethine chain. Excited-state optimizations were performed to identify possible emissive geometries. The results of these optimizations are presented in Figures 12 and 13 for IR140 and IR144, respectively. Three low-lying states were examined in both IR140 and IR144, which we will label S_1, S_1', and S_2. All structures were optimized in implicit solvents. Optimized structures for methanol, glycerol, and vacuum can be found in the Supporting Information.

The computed S_1 vertical excitation energies at the Franck−Condon (FC) point (S_0min) are 19 115 and 20 486 cm^{-1} for IR140 and IR144, respectively. These overestimate the respective experimental absorption maxima (12 421 and 13 469 cm^{-1} in methanol) by 6694 and 7017 cm^{-1}, respectively.

Thus, we apply respective shifts of the excited state potential energy surfaces of -6694 and -7017 cm^{-1} in our analysis of the computational data below. These shifts account both for well-known errors in TD-DFT excitation energies and for the different environment in our calculations compared with experiment (i.e., vibronic effects, conformational flexibility, the absence of charged sulfonate groups, counterions, and hydrogen bonding interactions with solvent).

The S_1 minimum was identified in each dye, which we label S_1min. In both cases, S_1min is very similar to S_0min and has a vertical S_0-S_1 gap less than 806 cm^{-1} smaller than that at S_0min. The shifted theoretical S_1 emission energies are in excellent agreement with experiment: 11 615 cm^{-1} (18309 cm^{-1} unshifted) and 12 179 cm^{-1} (19 196 cm^{-1} unshifted) for IR140 and IR144, respectively, compared to experimental values of 11 614 and 11 937 cm^{-1}. Optimization on S_1' did not yield a distinct minimum. Instead, it is found that S_1 and S_1' intersect, which likely facilitates efficient nonradiative decay from S_1' to S_1. Thus, no emission is expected from S_1'.

In both IR140 and IR144, two distinct local minima were found on S_2, which we label S_2min-1 and S_2min-2. As detailed below, in both systems, the computed S_0-S_2 energy gaps at these minima are in good agreement with the experimentally observed S_2^H and S_2^L emission peaks. In addition, in both IR140 and IR144, both S_2min-1 and S_2min-2 are significantly distorted compared to the S_0min structure. Of the two minima, S_2min-1 is more analogous to the Franck–Condon geometry; the polymethine chain remains planar, but the central amine group is twisted to 77° and 73° in IR140 and IR144, respectively (compared to 37° and 43° at S_0min). In the more distorted S_2min-2, the polymethine chain itself is twisted by 91° and 94°, relative to the planar S_0min structure. For comparison, the S_1min is less distorted, with a planar polymethine chain and respective twist angles about the central amine group of 50° and 59°.

These significant distortions of the emissive geometries compared to the S_1min structures explain the observed solvent viscosity dependence of the ratio of S_2 to S_1 emission in both IR140 and IR144. Upon excitation to the S_2 state, molecules will be trapped at the distorted S_2 minima by more viscous solvents and emit from S_2 before nonradiative decay can occur. Thus, the ratio between S_2 and S_1 emission intensity grows larger with increasing solvent viscosity.

Careful analysis of the S_2 PES sheds light on the origin of distinct S_2min-1 and S_2min-2 emission peaks. We believe that these two minima correspond to the experimentally observed S_2^H and S_2^L emission. In IR144, the predicted emission energies are 17 583 and 15 244 cm^{-1} (24 600 and 22 261 cm^{-1} unshifted) at S_2min-1 and S_2min-2, respectively. These values are in good agreement with the experimentally observed emission peaks at 17 150 and 15 890 cm^{-1}, respectively. Optimization in implicit methanol solvent provides nearly identical minima and emission energies. Thus, we suggest that S_2^H and S_2^L emission correspond to the excited state structures that are twisted about either the amine substituent or the polymethine chain, respectively.

For IR140 in glycerol, two distinct minima (S_2min-1 and S_2min-2) are observed as well. The computed emission energies are 21 213 and 16 776 cm^{-1} (27 907 and 23 471 cm^{-1} unshifted). These likely correspond to the experimentally observed S_2^H and S_2^L emission peaks at 17 230 and 15 900 cm^{-1}, though agreement with the computationally predicted feature at 21 213 cm^{-1} is only qualitative. In addition, only a single minimum (similar to S_2min-2) was observed upon optimization in implicit methanol solvent. Given the large

number of degrees of freedom on the molecule, there may be an additional minimum on S_2 that we have not found in our study. However, given the similarity of both the experimental emission spectra and the computed PESs of IR140 and IR144, it appears likely that the S_2^H and S_2^L emission peaks arise from distinct minima on S_2 in both systems.

Comparison of the S_2–S_1' energy gaps at the optimized S_2 minima provides insights into the relative ratios of S_2 to S_1 emission in these systems. In IR144, relatively small gaps of 4355 and 1694 cm^{-1} are predicted at the S_2min-1 and S_2min-2, respectively. This suggests relatively fast nonradiative relaxation to S_1', and subsequently to S_1 (through the above-mentioned intersection), which is consistent with the relatively low ratio of S_2 emission to S_1 emission in this system. The gaps are larger in IR140 (10082 and 5565 cm^{-1}), consistent with the higher yield of S_2 emission relative to S_1. The underlying raw calculations supporting the theory are provided in the Supporting Information Tables S5−S10 (Figures 12 and 13).

■ NUMERICAL SIMULATIONS

Numerical simulations were carried out to understand the chirp dependence observed experimentally, and how that dependence varies with the solvent viscosity and laser intensity. The simulations are based on the scheme shown in Figure 14.
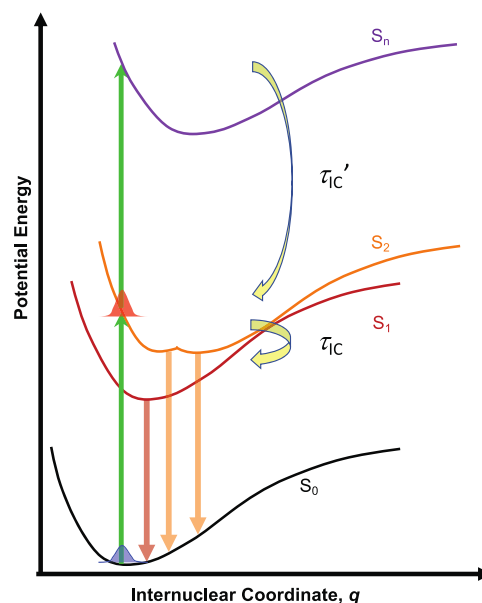
Figure 14. Schematic model representing potential energy curves that illustrate the different processes involved in the femtosecond chirped pulse experiments. As indicated in the Theory section, two S_2 states were identified. The S_2 state under the adiabatic representation can be considered as having a double well potential that leads to emission at two different wavelengths.

Before addressing the chirp dependence, the first goal was to simulate the fluorescence lifetime meaurements shown in Figures 7 and 8, whose fit parameters are listed in Table 1. For both molecules, we find that the fluorescence decay from S_2 shows biexponential behavior, with viscosity-dependent fast and slow components. Emission from S_1 shows an initial rise that does not vary significantly with viscosity followed by a single exponential decay. We thus assume that k_{IC} is independent of viscosity. Following the model in Figure 14, the first step is the excitation from S_0 to the FC region of S_2, forming the wave

packet shown in red. From there, the wave packet relaxes to either of the S_2 state configurations (S_2^H or S_2^L) with rate k_2 or crosses over to S_1, by way of a conical intersection between the two states, with an IC rate k_{IC}. The S_2 emission has two contributions, soon after excitation the population can be considered "hot" and is indicated as S_{2*}, following relaxation and a likely structural change as discussed in the quantum calculations presented above, emission is from a configuration that is much less likely to undergo IC, indicated as S_2. The simplest system of differential equations that describes the data is

$$\frac{d[S_{2*}]}{dt} = -(k_{IC}[S_{2*}] + k_2[S_{2*}] + k_{fl}[S_{2*}])$$

$$\frac{d[S_2]}{dt} = k_2[S_{2*}] - k_{fl}[S_2]$$

$$\frac{d[S_1]}{dt} = k_{IC}[S_{2*}] - k_{fl}[S_1]$$

$$(4)$$

The system of equations was solved using Mathematica, and the resulting equations for the populations are given in the Supporting Materials. For these calculations, the population starts in S_2 and the lifetimes associated with the rates $1/k_{IC}$ and $1/k_2$ are 32 and 46 ps, respectively, for methanol. To keep the model as compact as possible, we did not take into account the fact that some of the excitation goes directly into S_1 given that its higher vibrational states overlap with S_2, and we did not introduce the state $S_{1'}$, which is even closer to S_2. However, the initial excitation causes initial populations, which we designate S_{1_nat} and S_{2_nat}. No efforts were made to differentiate the model between IR144 and IR140. The fluorescence lifetimes for S_2 and S_1 were obtained from Table 1.

To simulate the chirp dependence results shown in Figure 9a, we include the possibility of two-photon excitation from the FC region reached by the first photon (linear superpositions of both S_1 and S_2 vibronic states) to a higher excited state (see Figure 14), which if such an excitation relaxes preferentially to S_2 explains the chirp dependence and the power dependence of the S_2 fluorescence shown in the Supporting Materials. When the pulses are TL, the probability of two-photon excitation is maximum, and as the chirp magnitude increases, the two-photon excitation is less probable. Two-photon excitation is proportional to pulse duration; thus, we set k_2 proportional to the inverse of the chirp-dependent pulse duration given by eq 1, such that for TL pulses k_2 decreases. We further note that the rate with which the molecular geometries associated with the S_{2L} and S_{2H} equilibrium, from which IC is no longer possible, is viscosity-dependent. This explains why the observed chirp dependence shown in Figure 9a,b becomes broader as viscosity increases. Therefore, we made k_2 proportional to viscosity divided by pulse duration. The time-integrated S_1 and S_2 populations as a function of chirp mimic the behavior, as observed in the experiments, without the need to introduce higher excited states or additional relaxation constants.

When the laser excitation is very weak, the effect of pulse chirp on fluorescence intensity becomes smaller, and in the limit where the photon density is such that the system dephases between each photon arrival, then the order or arrival of photons of higher or lower frequency, that is, the laser pulse chirp, no longer makes a difference, and the fluorescence intensity remains constant as a function of chirp. Because S_2 is nested within S_1 as illustrated in Figure 14 and because of the presence

of state S_1' as evidenced by the overlapping absorption spectra in Figure 4a,b, laser excitation populates both the S_1 and S_2 states. Empirically, we found that S_{1_nat} is 3.54 times greater than S_{2_nat}. With these observations and the viscosity values in Table 3, we were able to reproduce the chirp and viscosity dependence observed experimentally for methanol, ethanol, and propanol, as shown in Figure 15. For the simulations shown, the only parameter that was changed was the viscosity of the solvent.
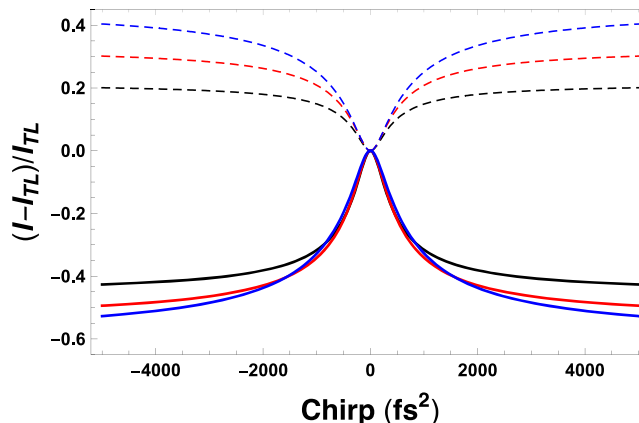

Figure 15. Results from numerical simulations of the S_1 and S_2 populations plotted as a function of chirp and viscosity. The viscosity of the solvent affects the rate k_2, and this is reflected in the chirp dependence. Results shown for methanol (black), ethanol (red), and propanol (blue), where the only parameter changed in these simulations was the viscosity of the solvent.

Saturation of the S_2 FC region occurs at high laser intensity in near-TL excitation conditions. In this case, as the pulse duration increases, the wave packet has time to move out of the FC region and S_2 can achieve a greater population than observed with TL pulses. As the pulse duration increases further, the behavior returns to the unsaturated case. Saturation was simulated by multiplying the S_2 population by a Gaussian function $\exp(-w^2)$, where $w = sk_2$. The saturation parameter s controls the extent of saturation. Because the rate constant k_2 is inversely proportional to pulse duration, we find that as the pulse duration increases because of chirp, the saturation decreases. The population of S_2 is also increased by any population in the FC region of S_1 before it relaxes. This contribution increases as the pulse duration increases at first, but then it decreases as the population relaxes and can no longer undergo two-photon excitation.

$$S_2 = e^{-w^2} \int_0^\infty S_2(t)dt + (1 - e^{-w^2}) \int_0^\infty S_1(t)S_{1\_nat}dt$$
$$+ S_{2\_nat}$$
$$(5)$$

The saturation parameter s goes from zero to 27 in our simulations. A plot of the simulations as a function of laser intensity, using the viscosity of methanol, are presented in Figure 16. At low intensities (blue line), the effect of chirp is minimal because two-photon excitation has a low probability. At optimum conditions, we observe a large relative difference as a function of chirp (red line). Under saturation conditions (black line), we observe that the population in the S_2 state increases above the TL value. The three conditions simulate the experimental data shown in Figure 10a. We did not include in our model the wave packet motion in the S_2 state that results in the asymmetry visible in the IR140 data (Figure 10b, namely
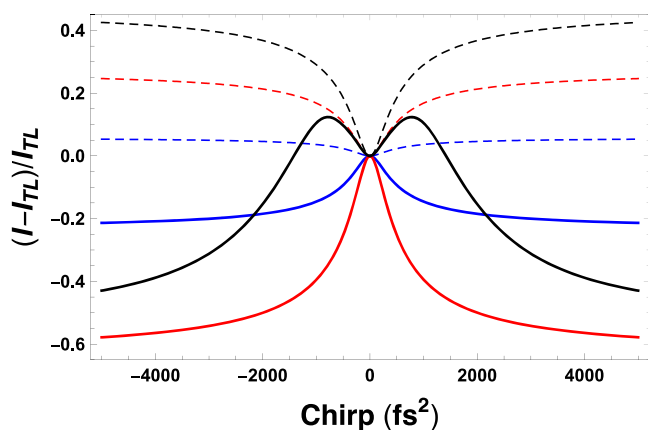
Figure 16. Results from numerical simulations of the S_1 and S_2 populations as a function of chirp for three different laser intensities: weak pulses (blue), higher intensity (red), and saturation (black); as described in the text.

that greater fluorescence intensity is observed for positively chirped pulses compared with negatively chirped pulses.

DISCUSSION

Results from steady-state spectroscopy, including EEM spectra and fluorescence lifetime measurements in IR144 and IR140 in different solvents, can be understood by taking advantage of the quantum calculations presented here. While emission from S_1 and S_2 states had been observed for both molecules before, here we report on a state we designate as S_1' that is bright in the sense of absorption but quickly decays to the bottom of the S_1 state. No evidence of S_1' fluorescence is observed in the EEM spectrum. Quantum calculations are able to predict this state and in addition find that it relaxes to the S_1 equilibrium geometry, consistent with experimental data. In addition, we report on two distinct molecular configurations for the S_2 state. These correspond to two different states with different molecular structure. Because of their close proximity in energy, excitation from the ground state populates both of these states. We find that IR144 is more likely to emit from S_2^H, but IR140 is more likely to emit from S_2^L. The preference can be explained by realizing that S_2^H is associated with twisting of the amine substituent, which is more easily accomplished for IR144 than IR140. Conversely, the bulky amine substituent in IR140 does not twist substantially, and emission from a configuration where the polymethine chain twists, corresponding to S_2^L, is preferred.

Fluorescence lifetime measurements report on the relatively long-lived S_2 states of these molecules, their dependence on viscosity, and their IC rate to the S_1 state. These measurements are later used to parametrize numerical simulations. The fluorescence decay from the S_2 states shows a biexponential behavior. We suggest that the biexponential decay arises from two sources. First, the initially excited "hot" population in S_2 is able to undergo IC and thus it has a fast fluorescence decay. Upon vibrational cooling and likely structural change as discussed in the quantum calculations, the relaxed S_2 state is much less likely to undergo IC, and it shows a fluorescence lifetime that is similar to the S_1 fluorescence lifetime.

Chirp-dependence measurements obtained following excitation of the S_2 state are very different than those obtained following excitation of the S_1 state.[24,26] The difference arises from two additional pathways. First, S_2 excitation can convert IC to the S_1 state and thus avoid depletion by negatively chirped

pulses. Second, resonance two-photon excitation to a higher state provides an additional source of signal for TL pulses. In the particular case of IR144 and to some extent in IR140, excitation with intense TL pulses increased the ratio of S_2 emission. The corresponding nonlinear optical Albrecht diagrams corresponding to S_1 and S_2 excitation are provided in the Introduction. In particular, pathway (2⁻) in Figure 2 is responsible for the depletion observe for negative chirps, and pathway (TPE) in Figure 3 is responsible for the enhancement observed for TL pulses. This was confirmed by power-dependence measurements and by fluorescence measurements under different laser excitation intensities.

The chirp dependence was found to broaden with solvent viscosity. This is because the initial motion of the wave packet, primarily due to intramolecular vibrational motion, is constrained by solvent viscosity. Therefore, as viscosity increases, the dependence on a fast chirp rate, which varies inversely with chirp magnitude, is less stringent. Moreover, as viscosity increases, the wave packet motion out of the FC region takes longer. This facilitates the two-photon excitation pathway, which apparently is not available once the wave packet has moved out of the FC region. We find that the slowdown is more pronounced for IR140 than for IR144, and this can be explained by the favored polymethine twist in IR144 as compared with the amine substituent twist in IR140.

At higher intensities, both molecules show saturation, such that one observes greater S_2 emission for chirped pulses than for TL pulses. The power dependence shows that IR140 is much more sensitive to saturation, as indicated by the magnitude of the chirp effect under intense pulse excitation. Interestingly, the S_1 chirp-dependent intensity does not show signs of saturation. We rationalize this observation by first noting that saturation depends on how the rate of excitation compares with the rate of wave packet motion out of the FC state. Direct excitation populates very high vibrational states in S_1 that undergo fast relaxation, which competes favorably against saturation. The fraction of the population in S_2 that undergoes IC to S_1 avoids saturation. Therefore, the two main sources of population to S_1 show no sign of saturation.

We confirmed that the S_2/S_1 ratio is maximized for TL pulses, as had been observed before by our group.[5] Most importantly, the enhanced S_2/S_1 ratio for TL pulses, as had already been reported by our group, can now be understood as a two-photon excitation originating from the FC region reached by the first photon, provided that the wave packet has not moved during the excitation process. This conclusion is reached by correlating multiple observations. First, two-photon 19 157 cm⁻¹ excitation (38 314 cm⁻¹ one-photon) leads to $S_2 \rightarrow S_0$ emission. Additional laser power dependence measurements are included in the SI (Figure S1). Numerical simulations based on a kinetic model allowed us to test several alternative processes and their dependence on laser intensity, pulse chirp, and solvent viscosity. The overall scheme depicted in Figure 14 is the one that was consistent with all our experimental observations.

One of the goals of this research was to take advantage of viscosity to slow intramolecular dynamics and enhance the population ratio S_2/S_1. The greater the S_2/S_1 ratio, the greater the probability to harness the photon energy provided by higher photon frequencies. Because in most molecules, excitation of higher states leads to very fast relaxation to the bottom of the first excited state, according to Kasha's rule, one is not able to take advantage of the full energy content of photons. Being able to populate long-lived higher excited states is essential to enable

novel photochemistry. For example, a cyanine derivative has recently been shown to undergo photodissociation following two-photon excitation to its second excited state.[56] One may extrapolate these results and imagine that capturing energy in higher excited states may lead to more efficient solar energy capture, especially systems containing cyanine compounds,[12] and perhaps theranostic applications whereby a compound excited to S_1 serves as fluorescent marker but when excited to S_2 serves as a therapy agent.

CONCLUSIONS

In this study, we have applied femtosecond pulse chirp and solvent viscosity to manipulate the rate of IC following S_2 excitation of IR144 and IR140. Steady-state spectroscopy including excitation emission spectra and fluorescence lifetime emission, together with quantum calculations have revealed an excited state termed $S_{1'}$, that promptly relaxes to S_1 but influences the IC process from S_2. In addition, we find that the S_2 state has two stable molecular configurations S_2^H and S_2^L associated with amine substituent twist or polymethine chain twist, respectively. We find that IR144 emits preferentially from S_2^H, while IR140 emits preferentially from S_2^L. By taking advantage of solvent viscosity and femtosecond pulse chirp, we are able to manipulate the S_2/S_1 fluorescence ratio of IR144 from a minimum value of 0.01 for methanol with 5000 fs^2 chirp, to a maximum of 0.86 obtained for TL pulses. This overall change corresponds to almost two-orders of magnitude. The ability to control IC from upper excited states, may open exciting possibilities for the photochemical applications of cyanine dyes in imaging and photodynamic therapy. The results presented here may lead to future work on manipulating the lifetime of the upper excited states of similar polymethine dyes, other cyanine dyes, and possibly other molecules such as carotenes.

ASSOCIATED CONTENT

Supporting Information

The Supporting Information is available free of charge at https://pubs.acs.org/doi/10.1021/acs.jpca.1c05772.

Laser intensity dependence of S_2 fluorescence; solvatochromic shifts of the S_2 state absorption and emission maxima for IR144 and IR140 in different alcohols; excitation spectrum detecting S_2 emission for IR144 and IR140 in different alcohols; solvent parameters; integrated fluorescence ratio (S_2/S_1) of IR144 and IR140 with varying solvent parameter including polarity, polarizability, and viscosity; extinction coefficient of IR144 and IR140 in different alcohols; fluorescence lifetime fitting; underlying raw calculations supporting the theory; optimized geometries; kinetic model used to simulate the fluorescence lifetime data (PDF)

Note: The data that support the findings of this study are available within the article and its Supporting Information. Further data are available from the corresponding author upon reasonable request.

AUTHOR INFORMATION

Corresponding Author

Marcos Dantus − *Department of Chemistry and Department of Physics and Astronomy, Michigan State University, East Lansing, Michigan 48824, United States;* orcid.org/0000-0003-4151-5441; Email: dantus@chemistry.msu.edu

Authors

Maryann Laboe − *Department of Chemical Engineering, Michigan State University, East Lansing, Michigan 48824, United States*

Jurick Lahiri − *Department of Chemistry, Michigan State University, East Lansing, Michigan 48824, United States;* orcid.org/0000-0002-2518-5617

Nila Mohan T. M. − *Department of Chemistry, Michigan State University, East Lansing, Michigan 48824, United States*

Fangchun Liang − *Institute for Advanced Computational Science and Department of Chemistry, Stony Brook University, Stony Brook, New York 11794, United States*

Benjamin G. Levine − *Institute for Advanced Computational Science and Department of Chemistry, Stony Brook University, Stony Brook, New York 11794, United States;* orcid.org/0000-0002-0356-0738

Warren F. Beck − *Department of Chemistry, Michigan State University, East Lansing, Michigan 48824, United States;* orcid.org/0000-0002-7491-0264

Complete contact information is available at:
https://pubs.acs.org/10.1021/acs.jpca.1c05772

Author Contributions

[#]M.L. and J.L. contributed equally to this work.

Notes

The authors declare no competing financial interest.

ACKNOWLEDGMENTS

REFERENCES

(1) Kasha, M. Characterization of Electronic Transitions in Complex Molecules. *Discuss. Faraday Soc.* **1950**, *9* (c), 14−19.

(2) Mohanty, J.; Palit, D. K.; Mittal, J. P. Photophysical Properties of Two Infrared Laser Dyes–IR-144 and IR-140: A Picosecond Laser Flash Photolysis Study. *Proc. Indian National Sci. Acad.* **2000**, *66 A*, 303−315.

(3) Goswami, D.; Das, D. K.; Makhal, K. Solvent Effect on Dual Fluorescence and the Corresponding Excited State Dynamics. In *Reviews in Fluorescence 2017*; Geddes, C. D., Lakowicz, J. R., Eds.; Reviews in Fluorescence; Springer: Cham, 2018; pp 145−160.

(4) Zhang, H.; Zhang, S.; Lu, C.; Jia, T.; Wang, Z.; Sun, Z. Single-Photon Fluorescence Enhancement in IR144 by Phase-Modulated Femtosecond Pulses. *Chem. Phys. Lett.* **2011**, *503* (1−3), 176−179.

(5) Nairat, M.; Konar, A.; Lozovoy, V. V.; Beck, W. F.; Blanchard, G. J.; Dantus, M. Controlling S_2 Population in Cyanine Dyes Using

Shaped Femtosecond Pulses. *J. Phys. Chem. A* **2016**, *120* (11), 1876−1885.

(6) Ballou, B.; Ernst, L. A.; Waggoner, A. S. Fluorescence Imaging of Tumors In Vivo. *Curr. Med. Chem.* **2005**, *12* (7), 795−805.

(7) Huang, B.; Jones, S. A.; Brandenburg, B.; Zhuang, X. Whole-Cell 3D STORM Reveals Interactions between Cellular Structures with Nanometer-Scale Resolution. *Nat. Methods* **2008**, *5* (12), 1047−1052.

(8) Pansare, V. J.; Hejazi, S.; Faenza, W. J.; Prud'homme, R. K. Review of Long-Wavelength Optical and NIR Imaging Materials: Contrast Agents, Fluorophores, and Multifunctional Nano Carriers. *Chem. Mater.* **2012**, *24* (5), 812−827.

(9) Zhang, Z.; Berezin, M. Y.; Kao, J. L. F.; d'Avignon, A.; Bai, M.; Achilefu, S. Near-Infrared Dichromic Fluorescent Carbocyanine Molecules. *Angew. Chem., Int. Ed.* **2008**, *47* (19), 3584−3587.

(10) Li, D.-H.; Schreiber, C. L.; Smith, B. D. Sterically Shielded Heptamethine Cyanine Dyes for Bioconjugation and High Performance Near-Infrared Fluorescence Imaging. *Angew. Chem., Int. Ed.* **2020**, *59* (29), 12154−12161.

(11) Sayama, K.; Tsukagoshi, S.; Mori, T.; Hara, K.; Ohga, Y.; Shinpou, A.; Abe, Y.; Suga, S.; Arakawa, H. Efficient Sensitization of Nanocrystalline TiO2 Films with Cyanine and Merocyanine Organic Dyes. *Sol. Energy Mater. Sol. Cells* **2003**, *80* (1), 47−71.

(12) Zhao, Y.; Meek, G. A.; Levine, B. G.; Lunt, R. R. Near-Infrared Harvesting Transparent Luminescent Solar Concentrators. *Adv. Opt. Mater.* **2014**, *2* (7), 606−611.

(13) Zhang, J.; Moemeni, M.; Yang, C.; Liang, F.; Peng, W.-T.; Levine, B. G.; Lunt, R. R.; Borhan, B. General Strategy for Tuning the Stokes Shifts of near Infrared Cyanine Dyes. *J. Mater. Chem. C* **2020**, *8* (47), 16769−16773.

(14) Delaey, E.; van Laar, F.; De Vos, D.; Kamuhabwa, A.; Jacobs, P.; de Witte, P. A Comparative Study of the Photosensitizing Characteristics of Some Cyanine Dyes. *J. Photochem. Photobiol., B* **2000**, *55* (1), 27−36.

(15) Conceição, D. S.; Ferreira, D. P.; Vieira Ferreira, L. F. Photochemistry and Cytotoxicity Evaluation of Heptamethinecyanine near Infrared (NIR) Dyes. *Int. J. Mol. Sci.* **2013**, *14* (9), 18557−18571.

(16) Shindy, H. A. Fundamentals in the Chemistry of Cyanine Dyes: A Review. *Dyes Pigm.* **2017**, *145*, 505−513.

(17) Bricks, J. L.; Kachkovskii, A. D.; Slominskii, Y. L.; Gerasov, A. O.; Popov, S. V. Molecular Design of near Infrared Polymethine Dyes: A Review. *Dyes Pigm.* **2015**, *121*, 238−255.

(18) Gunaratne, T. C.; Zhu, X.; Lozovoy, V. V.; Dantus, M. Symmetry of nonlinear optical response to time inversion of shaped femtosecond pulses as a clock of ultrafast dynamics. *Chem. Phys.* **2007**, *338*, 259−267.

(19) Bardeen, C. J.; Yakovlev, V. V.; Squier, J. A.; Wilson, K. R. Quantum Control of Population Transfer in Green Fluorescent Protein by Using Chirped Femtosecond Pulses. *J. Am. Chem. Soc.* **1998**, *120* (50), 13023−13027.

(20) Yakovlev, V. V.; Bardeen, C. J.; Che, J.; Cao, J.; Wilson, K. R. Chirped Pulse Enhancement of Multiphoton Absorption in Molecular Iodine. *J. Chem. Phys.* **1998**, *108* (6), 2309−2313.

(21) Mishima, K.; Hayashi, M.; Lin, J. T.; Yamashita, K.; Lin, S. H. A Numerical Study on Vibronic and Vibrational Dynamics Generated by Chirped Laser Pulses in the Presence of Relaxation Processes. *Chem. Phys. Lett.* **1999**, *309* (3−4), 279−286.

(22) Fainberg, B. D.; Narbaev, V. Chirped Pulse Excitation in Condensed Phases Involving Intramolecular Modes Studied by Double-Sided Feynman Diagrams for Fast Optical Dephasing. *J. Chem. Phys.* **2000**, *113* (18), 8113−8124.

(23) Misawa, K.; Kobayashi, T. Wave-Packet Dynamics in a Cyanine Dye Molecule Excited with Femtosecond Chirped Pulses. *J. Chem. Phys.* **2000**, *113* (17), 7546−7553.

(24) Konar, A.; Lozovoy, V. V.; Dantus, M. Solvent Environment Revealed by Positively Chirped Pulses. *J. Phys. Chem. Lett.* **2014**, *5*, 924−928.

(25) Nairat, M.; Webb, M.; Esch, M. P.; Lozovoy, V. V.; Levine, B. G.; Dantus, M. Time-Resolved Signatures across the Intramolecular Response in Substituted Cyanine Dyes. *Phys. Chem. Chem. Phys.* **2017**, *19* (21), 14085−14095.

(26) Konar, A.; Lozovoy, V. V.; Dantus, M. Solvation Stokes-Shift Dynamics Studied by Chirped Femtosecond Laser Pulses. *J. Phys. Chem. Lett.* **2012**, *3* (17), 2458−2464.

(27) Liebel, M.; Kukura, P. Lack of Evidence for Phase-Only Control of Retinal Photoisomerization in the Strict One-Photon Limit. *Nat. Chem.* **2017**, *9*, 45−49.

(28) Brühl, E.; Buckup, T.; Motzkus, M. Experimental and Numerical Investigation of a Phase-Only Control Mechanism in the Linear Intensity Regime. *J. Chem. Phys.* **2018**, *148*, 214310.

(29) Lozovoy, V. V.; Dantus, M. Laser control of Physicochemical Processes; Experiments and Applications. *Annu. Rep. Prog. Chem., Sect. C: Phys. Chem.* **2006**, *102*, 227−258.

(30) Mukamel, S. *Principles of Nonlinear Optical Spectroscopy*; Oxford University Press, 1995.

(31) Lee, D.; Albrecht, A. C. In *Advances in Infrared and Raman Spectroscopy*; Clark, R. J. H., Hester, R. E., Eds.; Wiley-Heyden: Chichester, U.K., 1985; Vol. *12*.

(32) Grimberg, I.; Lozovoy, V. V.; Dantus, M.; Mukamel, S. Femtosecond three-pulse spectroscopies in the gas phase: density matrix representation. *J. Phys. Chem. A* **2002**, *106*, 697−718.

(33) Cerullo, G.; Bardeen, C. J.; Wang, Q.; Shank, C. V. High-Power Femtosecond Chirped Pulse Excitation of Molecules in Solution. *Chem. Phys. Lett.* **1996**, *262*, 362−368.

(34) Nahmias, O.; Bismuth, O.; Shoshana, O.; Ruhman, S. Tracking Excited State Dynamics with Coherent Control: Automated Limiting of Population Transfer in LDS750. *J. Phys. Chem. A* **2005**, *109*, 8246−8253.

(35) Sharafy, S.; Muszkat, K. A. *J. Am. Chem. Soc.* **1971**, *93* (17), 4119−4125.

(36) Loutfy, R. O.; Arnold, B. A. Effect of viscosity and temperature on torsional relaxation of molecular rotors. *J. Phys. Chem.* **1982**, *86* (21), 4205−4211.

(37) Guarin, C. A.; Villabona-Monsalve, J. P.; López-Arteaga, R.; Peon, J. Dynamics of the Higher Lying Excited States of Cyanine Dyes. An Ultrafast Fluorescence Study. *J. Phys. Chem. B* **2013**, *117* (24), 7352−7362.

(38) Xu, B.; Gunn, J. M.; Dela Cruz, J. M.; Lozovoy, V. V.; Dantus, M. Quantitative Investigation of the Multiphoton Intrapulse Interference Phase Scan Method for Simultaneous Phase Measurement and Compensation of Femtosecond Laser Pulses. *J. Opt. Soc. Am. B* **2006**, *23* (4), 750.

(39) Coello, Y.; Lozovoy, V. V.; Gunaratne, T. C.; Xu, B.; Borukhovich, I.; Tseng, C.; Weinacht, T.; Dantus, M. Interference without an Interferometer: A Different Approach to Measuring, Compressing, and Shaping Ultrashort Laser Pulses. *J. Opt. Soc. Am. B* **2008**, *25* (6), A140.

(40) Lozovoy, V. V.; Rasskazov, G.; Pestov, D.; Dantus, M. Quantifying Noise in Ultrafast Laser Sources and Its Effect on Nonlinear Applications. *Opt. Express* **2015**, *23* (9), 12037.

(41) Birks, J. B.; Dyson, D. J. The Relations Between the Fluorescence and Absorption Properties of Organic Molecules. *Proc. R. Soc. London, Ser. A* **1963**, *275* (1360), 135−148.

(42) Angulo, G.; Grampp, G.; Rosspeintner, A. Recalling the Appropriate Representation of Electronic Spectra. *Spectrochim. Acta, Part A* **2006**, *65* (3−4), 727−731.

(43) Methanol - Dynamic and Kinematic Viscosity https://www.engineeringtoolbox.com/methanol-dynamic-kinematic-viscosity-temperature-pressure-d_2093.html.

(44) Ethanol - Dynamic and Kinematic Viscosity https://www.engineeringtoolbox.com/ethanol-dynamic-kinematic-viscosity-temperature-pressure-d_2071.html.

(45) Pang, F.-M.; Seng, C.-E.; Teng, T.-T.; Ibrahim, M. H. Densities and Viscosities of Aqueous Solutions of 1-Propanol and 2-Propanol at Temperatures from 293.15 to 333.15 K. *J. Mol. Liq.* **2007**, *136*, 71−78.

(46) Tsierkezos, N. G.; Molinou, I. E. Densities and Viscosities of Ethylene Glycol Binary Mixtures at 293.15 K. *J. Chem. Eng. Data* **1999**, *44*, 955−958.

(47) Segur, J. B.; Oberstar, H. E. Viscosity of Glycerol and Its Aqueous Solutions. *Ind. Eng. Chem.* **1951**, *43*, 2117−2120.

(48) Adamo, C.; Jacquemin, D. The Calculations of Excited-State Properties with Time-Dependent Density Functional Theory. *Chem. Soc. Rev.* **2013**, *42* (3), 845−856.

(49) Le Guennic, B.; Jacquemin, D. Taking Up the Cyanine Challenge with Quantum Tools. *Acc. Chem. Res.* **2015**, *48* (3), 530−537.

(50) Isborn, C. M.; Luehr, N.; Ufimtsev, I. S.; Martínez, T. J. Excited-State Electronic Structure with Configuration Interaction Singles and Tamm-Dancoff Time-Dependent Density Functional Theory on Graphical Processing Units. *J. Chem. Theory Comput.* **2011**, *7* (6), 1814−1823.

(51) Seritan, S.; Bannwarth, C.; Fales, B. S.; Hohenstein, E. G.; Isborn, C. M.; Kokkila-Schumacher, S. I. L.; Li, X.; Liu, F.; Luehr, N.; Snyder, J. W.; et al. TeraChem: A Graphical Processing Unit-Accelerated Electronic Structure Package for Large-Scale Ab Initio Molecular Dynamics. *Wiley Interdiscip. Rev.: Comput. Mol. Sci.* **2021**, *11* (2), 1−16.

(52) Ufimtsev, I. S.; Martinez, T. J. Quantum Chemistry on Graphical Processing Units. 3. Analytical Energy Gradients, Geometry Optimization, and First Principles Molecular Dynamics. *J. Chem. Theory Comput.* **2009**, *5* (10), 2619−2628.

(53) Yanai, T.; Tew, D. P.; Handy, N. C. A New Hybrid Exchange-Correlation Functional Using the Coulomb-Attenuating Method (CAM-B3LYP). *Chem. Phys. Lett.* **2004**, *393* (1−3), 51−57.

(54) Barone, V.; Cossi, M. Conductor Solvent Model. *J. Phys. Chem. A* **1998**, *102* (97), 1995−2001.

(55) Lange, A. W.; Herbert, J. M. A Smooth, Nonsingular, and Faithful Discretization Scheme for Polarizable Continuum Models: The Switching/Gaussian Approach. *J. Chem. Phys.* **2010**, *133* (24), 244111−18.

(56) Rodríguez-Romero, J.; Guarin, C. A.; Arroyo-Pieck, A.; Gutiérrez-Arzaluz, L.; López-Arteaga, R.; Cortés-Guzmán, F.; Navarro, P.; Peon, J. Fluorophore Release from a Polymethinic Photoremovable Protecting Group Through a Nonlinear Optical Process. *ChemPhotoChem.* **2017**, *1*, 397−407.